DEFORMATION BEHAVIOR OF A MAGNESIUM ALLOY SHEET WITH RANDOM CRYSTALLOGRAPHIC ORIENTATIONS UNDER VARIOUS LOADING PATHS

TAKAYUKI HAMA[1], TSUYOSHI MAYAMA[2], HIROHIKO TAKUDA[1]

Abstract. This paper reports deformation behavior under various loading paths at room temperature of a magnesium alloy sheet with random crystallographic orientations both experimentally and numerically. The flow stress under uniaxial tension was larger than that of uniaxial compression. When the sheet was subjected to reverse loading, a slightly sigmoidal curve occurred under compression followed by tension, whereas it did not occur under tension followed by compression. These results demonstrated that the sample showed a tension-compression asymmetry and a strain-path dependency as in the case of rolled Magnesium alloy sheets with strong basal texture. Results of crystal plasticity finite-element simulation depicted that these characteristics occurred because of a tension-compression asymmetry in twinning activity even in the sheet with random crystallographic orientations. These results exhibited that a tension-compression asymmetry and a strain-path dependency were inevitable in the deformation of magnesium alloys at room temperature irrespective of initial textures. An evolution of contour of plastic work was also investigated numerically to support this conclusion.

Keywords: cast magnesium alloy, crystal plasticity finite-element method, twinning, detwinning, yield locus, unloading, contour of plastic work.

1. INTRODUCTION

Magnesium (hereafter termed as Mg) alloys are the lightest metals that are utilized for structural components and they have attracted attention as lightweight materials for transport equipment because of an increasing demand to reduce CO_2 emission [1, 2]. Generally components made of Mg alloys are manufactured by die casting, thixoforming [3, 4], or sometimes warm forming of sheets [5, 6], but cold forming processes have rarely been utilized. This is because wrought Mg alloy sheets show a strong anisotropy in the deformation behavior and a poor drawability at room temperature. For instance, in rolled Mg alloy sheets the yield stress and the stress-strain curve are notably different between tension and compression [7–9].

[1] Department of Energy Science and Technology, Kyoto University
[2] Priority Organization for Innovation and Excellence, Kumamoto University

Ro. J. Techn. Sci. – Appl. Mechanics, Vol. 60, N^{os} 1–2, P. 24–38, Bucharest, 2015

They also exhibit a strong strain-path dependency: a sigmoidal curve occurs when the sheets are subjected to tension following compression, while such curve does not arise when they are subjected to compression following tension [7, 10, 11]. Moreover, rolled Mg alloy sheets can generally be elongated to a strain of approximately 0.2 under uniaxial tension, while they fracture at an initial stage of drawing processes [3, 5, 12]. These characteristic deformation behaviors hinder wide application of Mg alloy sheets.

Such characteristic deformations observed in Mg alloy sheets occur because of hexagonal close-packed (hcp) structure. Because the critical resolved shear stress (CRSS) is notably different depending on the slip systems, the hcp structure of Mg shows a strong crystal anisotropy [7, 13, 14]. At the same time, direction-dependent deformation twinning can be easily activated owing to its relatively small CRSS. Moreover, a strong basal texture is developed in rolled Mg alloy sheets; therefore, the effect of these anisotropic properties of hcp structure on macroscopic deformation becomes pronounced.

Recently, a lot of studies have been conducted to develop Mg alloy sheets with improved formability. Huang *et al*. [15] showed that a Mg alloy sheet obtained with warm rolling by a single differential speed rolling pass on a cast ingot yielded weak basal texture and relatively high stretchability. Kohzu *et al.* [16] reported that a weak basal texture could be attained using high-temperature annealing before and after the final rolling pass. Song *et al*. [17] depicted that repeated unidirectional bending followed by annealing at 260°C could weaken a basal texture significantly; thus, a larger elongation was attained. Cheng *et al*. [18] displayed that the equal channel angular rolling process yielded a Mg alloy sheet with nearly random crystallographic orientations and the sheet showed an improved drawability. Clearly, it is expected that a formability of Mg alloy sheets at room temperature can be improved by weakening the basal texture. In the abovementioned studies, the deformation behavior of the developed sheets was investigated in terms of drawability, stretchability, and uniaxial tensile test. It is needless to say that a sheet experiences various deformation modes such as biaxial loading and reverse loading during sheet metal forming. Therefore, it is important to understand deformation behavior of a sheet under various loading modes. However, comprehensive deformation behavior of a Mg alloy sheet with weak basal texture has not been investigated in detail.

In the present study, deformation behavior of a Mg alloy sheet that had random crystallographic orientations was investigated comprehensively both experimentally and numerically. In the experiment, a cast Mg alloy sheet was subjected to various strain paths such as tension, compression, tension followed by compression, and compression followed by tension, and the work-hardening behavior was studied. A crystal plasticity finite-element method (hereafter termed as FEM) was also used to examine the deformation mechanism of the cast Mg alloy sheet in detail. Furthermore, a contour of plastic work was also investigated

numerically. Some preliminary results were recently reported in an international conference proceedings paper [19]. In the present paper, comprehensive results and extensive discussion are described.

2. EXPERIMENTAL PROCEDURE

A cast AZ31 Mg alloy was used in the present study. Fig.1 shows the inverse pole figure of the sample measured using EBSD analysis. Random crystallographic orientations were attained in the sample as shown in Fig. 1. The average grain size was approximately 100 μm. A specimen with 1mm thickness shown in Fig. 2 was machined from a cast ingot. The specimen was annealed at 350°C for 1.5 h before testing. It should be noted that the geometry of sample was the same as that used in the experiment of a rolled Mg alloy sheet [11] to compare directly stress-strain curves between cast and rolled Mg alloy sheets. The deformation behavior at room temperature of the cast sheet was studied under monotonic tension, monotonic compression, tension followed by compression (hereafter termed as TC), and compression followed by tension (hereafter termed as CT). To prevent buckling during compression, comb-shaped dies were utilized to impart a compressive force in the thickness direction of the sample [10, 20]. The magnitude of the compressive force in the thickness direction was 5 kN. This force was equivalent to the through-thickness stress of approximately 1 MPa and to approximately 1% of the 0.2% proof stress of the sample. Mineral hydraulic oil was used as a lubricant between the comb-shaped dies and the sample. It should be noted that the comb-shaped dies were employed also in the monotonic tension test to unify the experimental conditions.

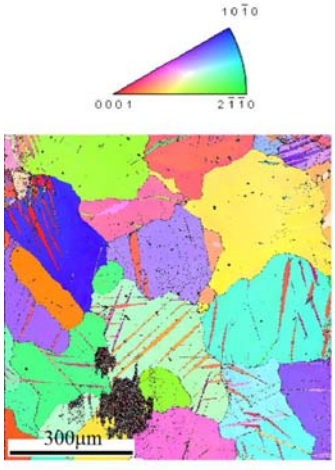

Fig. 1 – Inverse pole figure of sample.

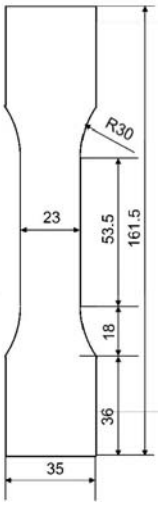

Fig. 2 – Geometry of specimen in mm.

The tests were performed at an initial strain rate of $6.67\times10^{-4}/s^{-1}$. Strains were measured using a strain gauge (Kyowa Electronic Instruments, KFEM). The experimental data were recorded approximately every 10 ms.

3. CRYSTAL PLASTICITY FINITE-ELEMENT METHOD

Crystal plasticity models are useful to analyze the relationship between macroscopic and mesoscopic crystalline deformations in metals. Nowadays the models are often used to analyze deformation behavior of magnesium alloys [21–24]. In the present study, a crystal plasticity FEM employed also in our previous studies [25–28] was used. In this section the model is described briefly. For detailed information on the crystal plasticity FEM, the reader is referred to the literatures [25–28].

To model the mechanical deformation behavior of Mg alloy, families of basal <a> slip, prismatic <a> slip, and pyramidal <a+c> slip and a family of $\{1\ 0\ \bar{1}\ 2\}$ tension twinning are taken into consideration [29]. First a model of slip deformation is described. Assuming that Schmid's law holds in each crystalline slip, the slip rate $\dot{\gamma}^{(\alpha)}$ of the α-slip system is given by the following viscoplastic power law

$$\frac{\dot{\gamma}^{(\alpha)}}{\dot{\gamma}_0}=\left|\frac{\tau^{(\alpha)}}{\tau_Y^{(\alpha)}}\right|^{\frac{1}{m}}\operatorname{sign}\left(\tau^{(\alpha)}\right),\quad \tau^{(\alpha)}=\mathbf{s}^{(\alpha)}\cdot\boldsymbol{\sigma}\cdot\mathbf{m}^{(\alpha)}, \tag{1}$$

where $\tau^{(\alpha)}$ is the Schmid's resolved shear stress, $\tau_Y^{(\alpha)}$ is the slip resistance of the α-slip system, $\dot{\gamma}_0$ is the reference strain rate, m is the rate-sensitivity exponent, and $\mathbf{s}^{(\alpha)}$ and $\mathbf{m}^{(\alpha)}$ are the unit vectors representing the slip direction and the slip plane normal, respectively. It should be noted that kinematic hardening is not taken into account for the sake of simplicity although reverse loading is studied in the present study. This assumption is employed because in our previous studies stress-strain curves under reverse loading in a rolled Mg alloy sheet could be predicted well without considering kinematic hardening. In fact, a kinematic hardening model that can be used in the framework of crystal plasticity FEM has rarely been established in particular for hcp structure having a strong crystal anisotropy. Therefore, the consideration of kinematic hardening will be our future work.

The rate of increase of $\tau_Y^{(\alpha)}$ owing to work-hardening is given in the form

$$\dot{\tau}_Y^{(\alpha)}=\sum_{\beta}q_{\alpha\beta}h\left|\dot{\gamma}^{(\beta)}\right|, \tag{2}$$

where $q_{\alpha\beta}$ with $\alpha=\beta$ and with $\alpha\neq\beta$ are the self- and latent-hardening moduli, respectively, and h is the hardening rate. The following linear hardening and Voce hardening are assumed for the basal slip and the nonbasal slip, respectively

$$h = h_0 \tag{3}$$

and

$$h = h_0\left(1-\frac{\tau_0}{\tau_\infty}\right)\exp\left(-\frac{h_0\bar{\gamma}}{\tau_\infty}\right) \quad \text{with } \bar{\gamma}=\sum_\alpha\int\left|\dot{\gamma}^{(\alpha)}\right|\mathrm{d}t\,, \tag{4}$$

where $\bar{\gamma}$ is the cumulative shear strain on all slip systems and τ_0 is the initial strength of slip resistance $\tau^{(\alpha)}$. h_0 and τ_∞ are the material parameters.

A twinning model originally proposed by Van Houtte [30] and a detwinning model recently proposed by the authors [27, 28] are employed. The models assume that shear strain rate induced by the activity of α-twinning system is described using eq. (1) as in the case of slip activity. The expansion of twinned region in each grain is modelled by the increase of $\tau_Y^{(\alpha)}$ using eqs. (2) and (3). The lattice rotation due to twinning is modelled using a statistical way as follows. The volume fraction of α-twinning system $f^{(\alpha)}=\bar{\gamma}_{\text{twin}}^{(\alpha)}/\gamma_{\text{ref}}$, with $\bar{\gamma}_{\text{twin}}^{(\alpha)}$ and γ_{ref} being the cumulative shear strain induced by twinning and the reference shear strain, respectively, is calculated each time increment. All slip systems are rotated with regard to α-twinning system when $f^{(\alpha)}$ exceeds a threshold value $f_{\text{th}}^{(\alpha)}$ which is determined pseudo-randomly before the calculation. A similar procedure is utilized for detwinning.

A static FEM [31] is used in which explicit time integration is employed with the aid of the rate tangent modulus method [32]. $r_{\min}$-strategy is also used to prevent an increase of the nonequilibrated forces [33–35]. The abovementioned crystal plasticity model is incorporated into each Gauss point in finite elements.

A finite-element model used in the present study is a cube with a length of 10 mm. The cube is divided into 10 uniform 8-node brick elements in each direction. Selective reduced integration is utilized. Initial random crystallographic orientations are artificially created and assigned to the model. It should be noted that a same orientation is assigned to all Gauss points in an element; thus, there are 1000 initial orientations.

To simulate the deformation behavior under uniaxial loading, the planes $x=0$, $y=0$, and $z=0$ of the finite-element model are fixed in the x, y, and z directions, respectively, and small displacement increments are imparted to the plane $x=10$.

4. IDENTIFICATION OF MATERIAL PARAMETERS

Because the CRSS and the work-hardening are different depending on the families of slip or twinning systems in Mg alloys as described before, the number of material parameters to be determined is large; thus, it is difficult of identify them properly. In our previous paper [36], a procedure has been proposed to identify the material parameters separately for each slip or twinning systems in rolled Mg alloy sheets. Because this procedure takes into account the deformation characteristics of rolled sheets with strong basal texture, it cannot be applied to Mg alloys with weak texture or even random orientations. In the present study, the material parameters for the cast Mg alloy sheet were identified under the following strong assumptions.

First it was assumed that the parameters previously identified for a rolled AZ31 Mg alloy sheet were also applicable to the cast AZ31 Mg alloy sheet. On the other hand, the grain sizes for the rolled and cast sheets were approximately 20 and 100 μm, respectively; thus, the effect of difference in grain size on the material parameters should also be taken into account. Therefore, it was further presumed that the Hall-Petch law was applicable to the CRSS τ_0. Following a literature [37], the Hall-Petch law for AZ31 Mg alloys is given as follows

$$\sigma_{0.2\%} = 127 + 0.17 d^{-1/2}, \tag{1}$$

where $\sigma_{0.2\%}$ is the 0.2% proof stress and d is the grain size. Using the parameters identified for the rolled Mg alloy sheet [38] and eq.(1) yielded the parameters for the cast Mg alloy sheet shown in Table 1. It should be noted that the work-hardening parameters were assumed to be the same as those of the rolled sheet although they would also be dependent on grain size. This assumption was owing to lack of experimental data for the Hall-Petch law. Following our previous study, the rest of parameters was assumed as follows: Young's modulus $E = 42$ GPa, Poisson's ratio $\nu = 0.3$, the rate sensitivity exponent $m = 0.02$, the reference strain rate $\dot{\gamma}_0 = 0.001\ \mathrm{s}^{-1}$, and the reference shear strain $\gamma_{\mathrm{ref}} = 0.16$. The parameters reported in a literature [29] was utilized for $q_{\alpha\beta}$.

Table 1

Identified material parameters

	Basal	Prismatic	Pyramidal-2	Twinning
τ_0 /MPa	8.23	82.3	82.3	37.5
τ_∞ /MPa	-	726	365	-
h_0 /MPa	30	950	530	60

5. RESULTS AND DISCUSSION

5.1. STRESS-STRAIN CURVES UNDER VARIOUS STRAIN PATHS

Figure 3 shows the stress-strain curves under monotonic tension and compression obtained from the experiment and the simulation. It should be noted that absolute strain and stress are used to compare the results directly between tension and compression. The experimental results of a rolled Mg alloy sheet are also displayed for reference. An asymmetry in the curves between tension and compression is pronounced in the rolled sheet, while it is much less pronounced in the cast sheet. However, the flow stress under tension is larger than that of compression also in the cast sheet, exhibiting a moderate asymmetry. The asymmetry in the flow stress observed in the cast sheet is predicted well in the simulation results.

Figure 4 shows the stress-strain curves obtained under CT and TC. 2% and 4% shown in the legends represent the magnitudes of strain imparted during the first loading. The signs of stress and strain in the results of TC are inverted to compare with the results of CT directly. A strong strain-path dependency occurs in the rolled sheet: a sigmoidal curve is exhibited during tension under CT, whereas such tendency is hardly visible during compression under TC. A similar tendency is also observed in the cast sheet although the sigmoidal curve under CT is much less pronounced. The sigmoidal curve under CT is smaller for 4% CT than 2% CT and this tendency is consistent with that observed in the rolled sheet [11, 38]. To examine the strain-path dependency in the cast sheet in detail, Fig. 5 depicts the transitions of instantaneous gradient of stress-strain curve as a function of strain after the loading direction was inverted. In the case of CT (Figs. 5a and 5b), the gradient decreases sharply just after the loading direction is inverted to tension and

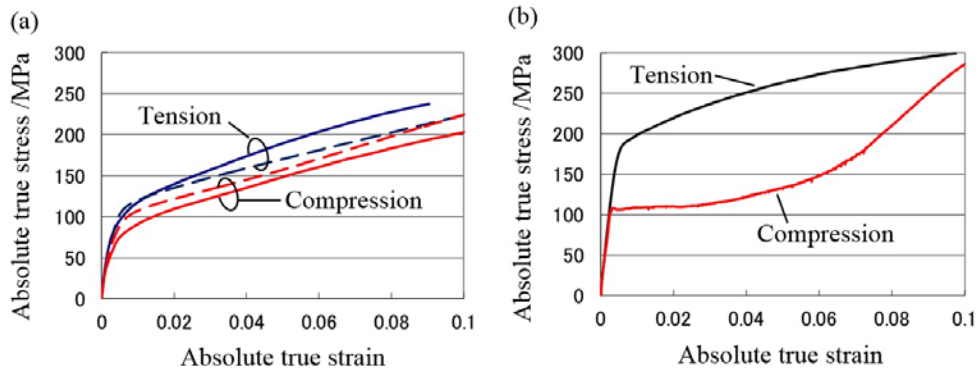

Fig. 3 – Absolute true stress-absolute true strain curves obtained under uniaxial tension and compression: a) cast sheet; b) rolled sheet. The solid and dotted lines are experimental and simulation results, respectively.

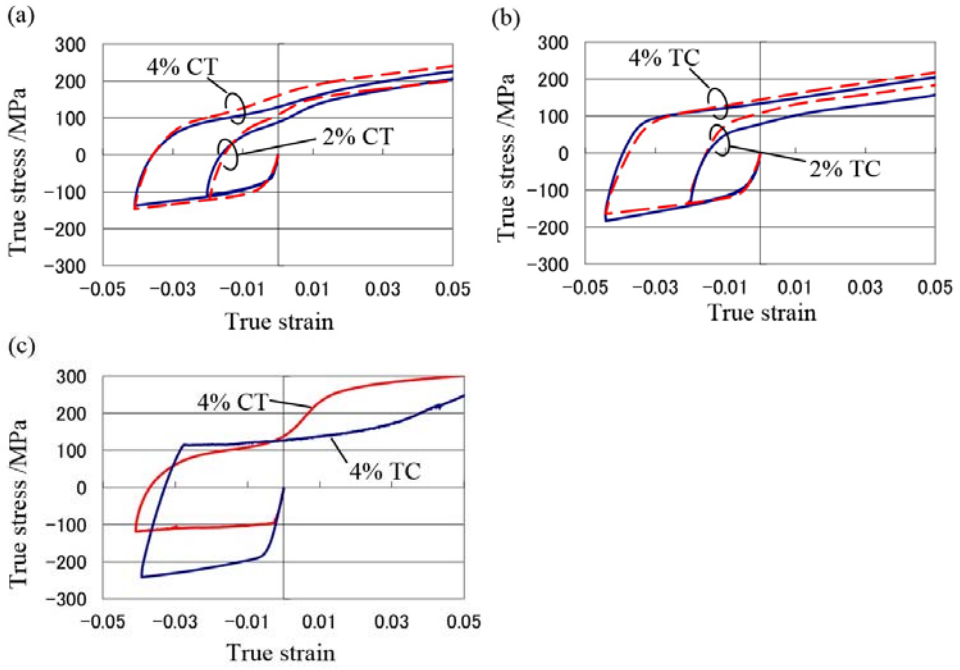

Fig. 4 – True stress-true strain curves obtained under reverse loading tests: a) CT results of cast sheet; b) TC results of cast sheet; c) CT and TC results of rolled sheet. The solid and dotted lines are experimental and simulation results, respectively. The signs of stress and strain in TC results are inverted.

then it increases gradually in the vicinity of strain of zero, and finally decreases gradually again. The increasing tendency is more pronounced in the result of 2% CT. On the other hand, such tendency is much less pronounced under 2% TC and even it is not exhibited under 4% TC. The results of simulation in Figs. 4 and 5 are qualitatively in good agreement with the experimental results regardless of the strain paths.

The aforementioned results display that a tension-compression asymmetry and a strain-path dependency obviously occur in the cast sheet although they are much less pronounced than those of the rolled sheet. Moreover, despite the rough parameter identification, the results of crystal plasticity analysis capture the characteristics observed in the experimental results well.

The simulation results are used to investigate the mechanism of the asymmetry and the strain-path dependency observed in the cast sheet. Figure 6 shows the transition of relative activity as a function of accumulated absolute strain. The relative activity of each family of slip or twinning systems r_i is given in the form

$$r_i = \sum_{n_s}^{n} \sum_{k} \left| \Delta\gamma^{(n_s,k)} \right| \Big/ \sum_{n_s}^{n} \sum_{j} \left| \Delta\gamma^{(n_s,j)} \right|, \tag{2}$$

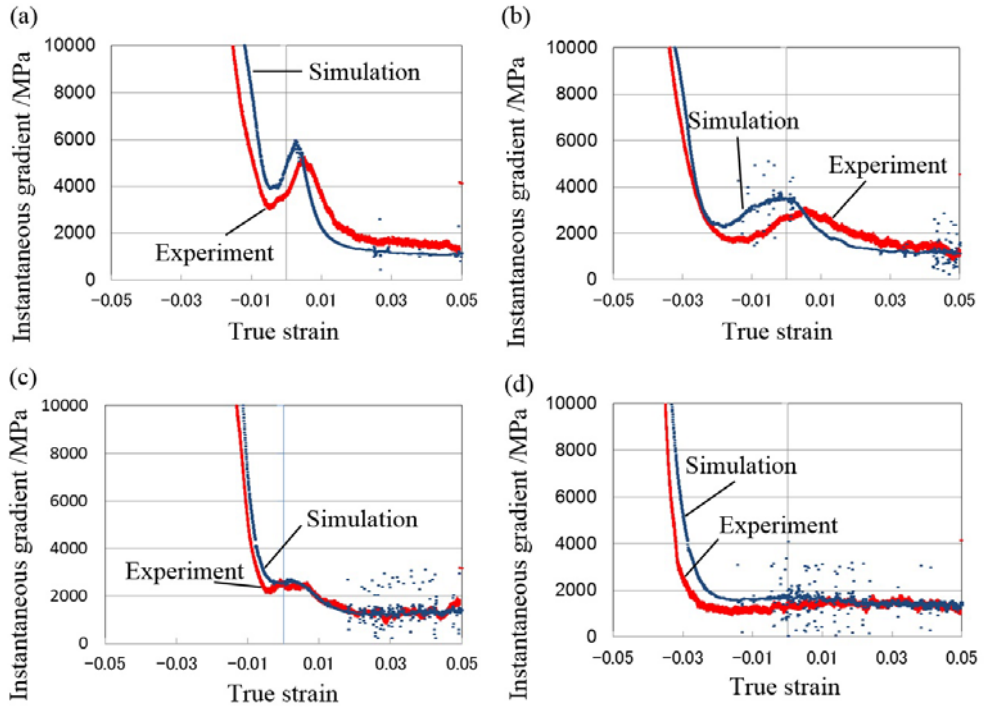

Fig. 5 – Transition of instantaneous gradient after the loading direction is inverted: a) 2% CT ; b) 4% CT; c) 2% TC ; d) 4% TC. The signs of stress and strain in TC results are inverted.

where the numerator is the plastic strain increment contributed by the family of slip or twinning systems *i*, summed over all grains. *k* is the number of slip or twinning systems of the family *i*. The denominator is the plastic strain increment contributed by all families, summed over all the grains. *j* is the total number of slip and twinning systems. Twinning and detwinning are evaluated separately. For reference, the transition of instantaneous gradient depicted in Fig. 5 is also shown. The result of 4% CT is as follows. During compression, the activity of basal slip is the largest and the twinning activity is the second largest among the systems. The activities of prismatic slip and pyramidal <a+c> slip are also observed. After the loading direction is inverted to tension, detwinning exhibits the second largest activity in the initial stage of tension. The detwinning activity then decreases gradually and at the same time the activities of prismatic slip and pyramidal <a+c> slip increase gradually. The increasing tendency in the transition of instantaneous gradient in the initial stage of tension is synchronized with the activities of prismatic slip and pyramidal <a+c> slip. In the latter stage of tension, the activity of prismatic slip becomes the second largest. The aforementioned results are similar to those observed in a rolled sheet subjected to CT [27].

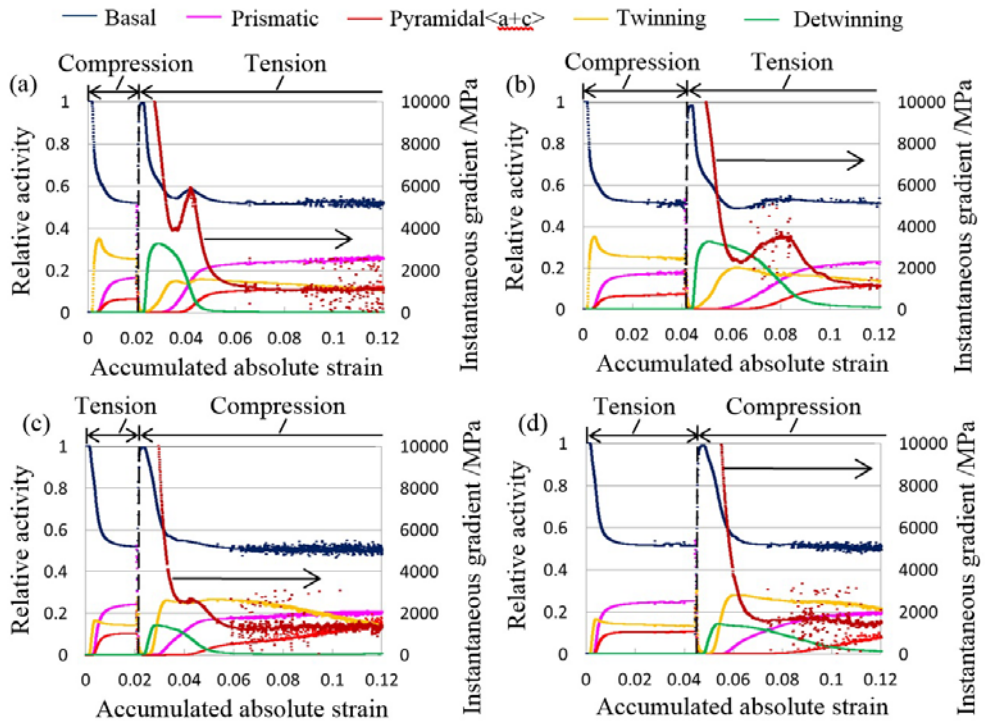

Fig. 6 – Transition of relative activities during cyclic loading: a) 2% CT, b) 4% CT ; c) 2% TC; d) 4% TC.

It is understood that the sigmoidal curve in a rolled sheet occurs because of a change in detwinning activity, consistent with the results observed in Fig. 6(b).

The tendency of activities observed in 2% CT is qualitatively the same as that of 4% CT. On the other hand, the decreasing and increasing tendencies of detwinning and nonbasal slip activities, respectively, are sharper than those of 4% CT, yielding the pronounced sigmoidal stress-strain curve.

In the case of TC, the activities of twinning and detwinning are obviously different from those under CT for both 2% and 4% conditions. The twinning activity during tension is smaller than that during compression under CT. As a result, the detwinning activity after the loading direction is inverted is also smaller under TC than CT; thus, a sigmoidal shape in the stress-strain curves is less pronounced. The tension-compression asymmetry in the twinning activity observed in Fig. 6 is similar to that of rolled sheets [25, 28] although the asymmetry is much more moderate in the cast sheet. The above results indicate that the asymmetry in stress-strain curve is inevitable due to the asymmetry in twinning activity irrespective of textures in Mg alloy sheets. The mechanism that the twinning

activity is larger under compression than tension despite the random crystallographic orientations would be that there is greater frequency of an occasion where tensile stress acts on the *c*-axes of hcp structure under compression than tension [39].

5.2. CONTOUR OF PLASTIC WORK

The aforementioned results further suggest that an isotropic work-hardening behavior cannot be expected also in biaxial stress conditions in the cast sheet. To support this presumption, an evolution of contour of plastic work in the cast sheet is investigated numerically. The simulation procedure is the same as that used in our previous study [26]. Figure 7 depicts the contours obtained using the crystal plasticity analysis. The contours are normalized using the uniaxial stress in the *x* direction σ_0. ε_0^p in the legend represents the uniaxial plastic strain in the *x* direction. To examine anisotropy of the contours, the von Mises isotropic yield locus is also shown by the dotted line for reference. The initial contour already displays a moderate anisotropy: the stresses in the vicinity of equibiaxial stress conditions are smaller than the von Mises locus. The normalized stresses in the region of biaxial tension remain nearly unchanged, exhibiting that the work-hardening is nearly isotropic. This tendency is different from that observed in a rolled sheet where a strong anisotropic work-hardening occurs [26, 40]. On the other hand, relatively large anisotropic work-hardening is exhibited in the vicinity of equibiaxial compression. More specifically, the contour in the third quadrant shrinks notably just after the plastic deformation begins and then it expands very gradually.

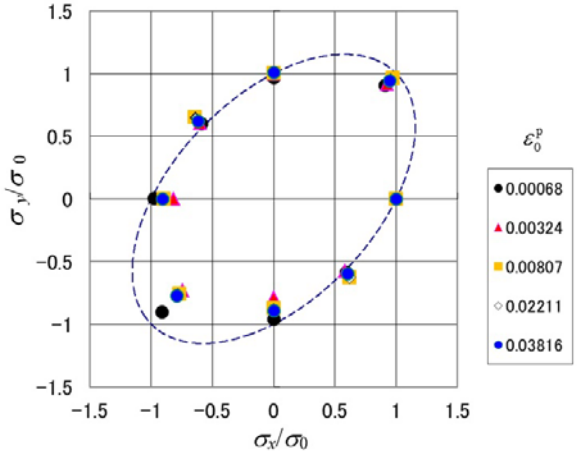

Fig. 7 – Normalized contour of plastic work obtained from simulation. Contours are normalized using the uniaxial stress in the *x* direction σ_0. The dotted line represents the von Mises yield locus. ε_0^p denotes the uniaxial plastic strain in the *x* direction.

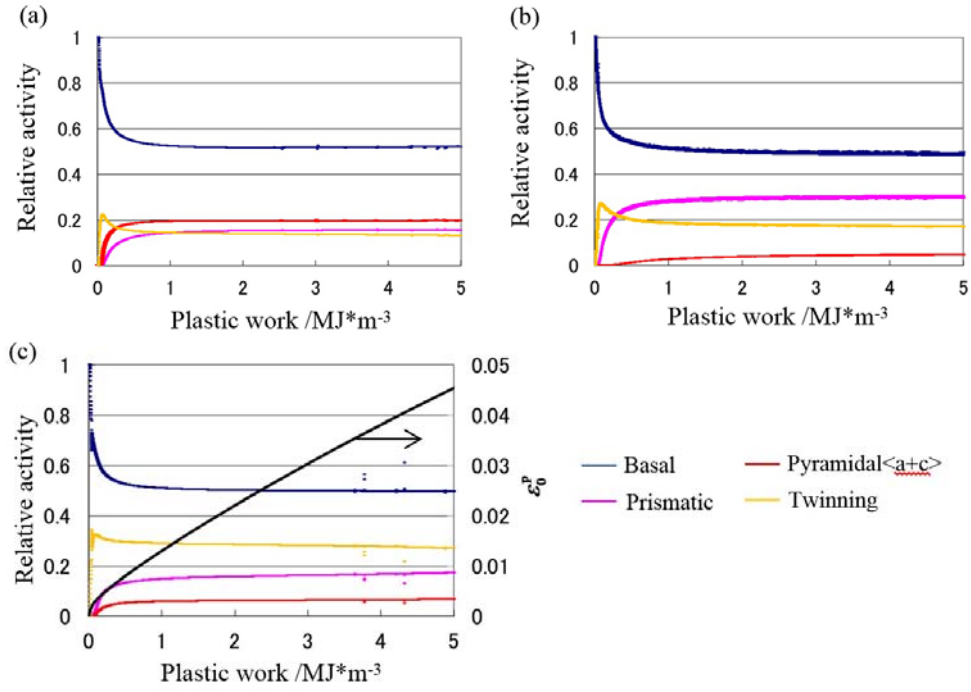

Fig. 8 – Transition of relative activities under stress ratios of: a) 1:1; b) –1:1; c) –1:–1.

The difference in the work-hardening behavior between biaxial tension and biaxial compression may also be because of the asymmetry of twinning activity. To confirm this presumption, Fig. 8 shows the evolutions of relative activities as a function of plastic work under the stress ratios σ_x:σ_y =1:1, –1:1, and –1:–1. The relationship between ε_0^p and the plastic work is displayed in Fig. 8c. The results under σ_x:σ_y =1:0 and –1:0 are not shown here because similar results are already exhibited in Fig. 6. The twinning activities under σ_x:σ_y =1:1, –1:1, and –1:–1 at the plastic work of approximately 3.0 are approximately 13%, 17%, and 28%, respectively. Obviously, the twinning activity becomes large as the biaxial stress condition moves from the first to third quadrants as we expected. This result indicates that the flow stress under the biaxial compression is smaller than that of the biaxial tension as in the cases of uniaxial tension and compression (Fig. 3); thus, the anisotropic work-hardening arises in the contours even in the cast sheet. It is interesting that the activity of pyramidal <a+c> slip is much larger under σ_x:σ_y=1:1 than that under σ_x:σ_y=–1:–1 and –1:1. A similar tendency was also observed in a rolled sheet [26]. This large activity of pyramidal <a+c> slip occurs under σ_x:σ_y =1:1 for the following two factors: (a) prismatic slip becomes more difficult to activate as the stress ratio approaches 1:1. This is because σ_x and σ_y tend to cancel each other; thus, the resolved shear stress becomes small. And (b)

the Schmid factors of the pyramidal <a+c> slip are relatively high in the vicinity of equibiaxial tension; thus, the activity of pyramidal <a+c> slip becomes large instead of prismatic slip. On the other hand, the aforementioned mechanisms do not hold in the vicinity of equibiaxial compression. This is because the primary activity under compression is twinning and its activity further increases as the stress ratio approaches −1:−1; thus, the activity of pyramidal <a+c> slip is not necessary. This result exhibits that the asymmetric work-hardening occurs owing to the difference in not only the twinning activity but also the nonbasal slip activities. These results further confirm the conclusion that the tension-compression asymmetry in deformation behavior is inevitable even in Mg alloy sheets with random crystallographic orientations. Moreover, it is suggested to employ an anisotropic yield function [e.g. 41] when the deformation behavior of Mg alloys is modeled irrespective of the initial crystallographic orientations.

6. CONCLUSION

The effect of randomization of crystallographic orientations in magnesium alloys on deformation behavior is investigated in the present study. To this end, deformation behavior under various loading paths in a cast magnesium alloy sheet with random crystallographic orientations was studied both experimentally and numerically. The results obtained in this work are summarized as follows.

(1) The cast sheet shows asymmetric work-hardening behavior between tension and compression: the flow stress is larger under tension than compression. Moreover, the cast sheet exhibits a strain-path dependency in the work-hardening: a sigmoidal curve occurs under compression followed by tension, whereas it is hardly visible under tension followed by compression.

(2) The above asymmetry and strain-path dependency can be predicted well using a crystal plasticity finite-element method. The simulation results indicate that the aforementioned anisotropic deformation behavior would be because of the fact that the twinning activity is larger under compression than under tension.

(3) An evolution of contour of plastic work in the cast sheet is investigated numerically. The contour of plastic work obviously shows anisotropic work-hardening behavior between biaxial tension and biaxial compression. The above results describe that the asymmetric deformation behavior between tension and compression is inevitable even in Mg alloy sheets with random crystallographic orientations.

Acknowledgements. This work was partially supported by Japan Society for the Promotion of Science KAKENHI Grant number 26289271 and the Photon and Quantum Basic Research Coordinated Development Program from the Ministry of Education, Culture, Sports, Science and Technology, Japan.

Received on April 23, 2015

REFERENCES

1. DOEGE, E., DRODER, K., *Sheet metal forming of magnesium wrought alloy – formability and process technology*, J. Mater. Process. Technol., **115**, *1*, pp. 14–19, 2001.
2. KULEKCI, M.K., *Magnesium and its alloys applications in automotive industry*, Int. J. Adv. Manuf. Technol., **39**, *9–10*, pp. 851–865, 2008.
3. LEE, Y.S., KIM, M.C., KIM, S.W., KWON, Y.N., CHOI, S.W., LEE, J.H., *Experimental and analytical studies for forming limit of AZ31 alloy on warm sheet metal forming*, J. Mater. Process. Technol., **187–188**, pp. 103–107, 2007.
4. KANEKO, J., SUGAMATA, M., *Mechanical properties and formability of magnesium alloy sheets* (in Japanese), J. Japan Inst. Light Metals, **54**, *11*, pp. 484–492, 2004.
5. CHEN, F.K., HUANG, T.B., CHANG, C.K., *Deep drawing of square cups with magnesium alloy AZ31 sheets*, Int. J. Mach. Tool. Manu., **43**, *15*, pp. 1553–1559, 2003.
6. HAMA, T., KARIYAZAKI, Y., OCHI, K., FUJIMOTO, H., TAKUDA, H., *Springback characteristics of magnesium alloy sheet AZ31B in draw-bending*, Mater. Trans., **51**, *4*, pp. 685–693, 2010.
7. LOU, X.Y., LI, M., BOGER, R.K., AGNEW, S.R., WAGONER, R.H., *Hardening evolution of AZ31B Mg sheet*, Int. J. Plast. **23**, *1*, pp. 44–86, 2007.
8. CHINO, Y., KIMURA, K., MABUCHI, M., *Twinning behavior and deformation mechanisms of extruded AZ31 Mg alloy*, Mater. Sci. Eng. A, **486**, pp. 481–488, 2008.
9. HAMA, T., KITAMURA, N., OCHI, K., FUJIMOTO, H., TAKUDA, H., *Unloading behavior of a magnesium alloy sheet under various loading paths*, Steel Res. Int., Special edition, pp. 1054–1059, 2011.
10. HAMA, T., KARIYAZAKI, Y., HOSOKAWA, N., FUJIMOTO, H., TAKUDA, H., *Work-hardening behaviors of magnesium alloy sheet during in-plane cyclic loading*, Mater. Sci. Eng. A, **551**, pp. 209-217, 2012.
11. HAMA, T., NAGAO, H., KUCHINOMACHI, Y., TAKUDA, H., *Effect of pre-strain on work-hardening behavior of magnesium alloy sheets upon cyclic loading*, Mater. Sci. Eng. A, **591**, pp. 69–77, 2014.
12. KIMA, H.J., CHOI, S.C., LEE, K.T., KIMA, H.Y., *Experimental Determination of Forming Limit Diagram and Springback Characteristics of AZ31B Mg Alloy Sheets at Elevated Temperatures*, Mater. Trans., **49**, *5*, pp. 1112–1119, 2008.
13. AGNEW, S.R., DUYGULU, O., *Plastic anisotropy and the role of nonbasal slip in magnesium alloy AZ31B*, Int. J. Plast., **21**, *6*, pp. 1161–1193, 2005.
14. KOIKE, J., *Enhanced deformation mechanisms by anisotropic plasticity in polycrystalline Mg alloys at room temperature*, Metall. Mater. Trans. A, **36**, *7*, pp. 1689–1696, 2005.
15. HUANG, X., SUZUKI, K., YUASA, M., CHINO, Y., *Effects of initial microstructure on the microstructural evolution and stretch formability of warm rolled Mg-3Al-1Zn alloy sheets*, Mater. Sci. Eng. A, **587**, pp. 150–160, 2013.
16. KOHZU, M., KII, K., NAGATA, Y., NISHIO, H., HIGASHI, K., INOUE, H., *Texture randomization of AZ31 Magnesium alloy sheets for improving the cold formability by a combination of rolling and high-temperature annealing*, Mater. Trans., **51**, *4*, pp. 749–755, 2010.
17. SONG, B., HUANG, G., LI, H., ZHANG, L., HUANG, G., PAN, F., *Texture evolution and mechanical properties of AZ31B magnesium alloy sheets processed by repeated unidirectional bending*, J. Alloys Compd., **489**, *2*, pp. 475–481, 2010.
18. CHENG, Y.Q., CHEN, Z.H., XIA, W.J., *Drawability of AZ31 magnesium alloy sheet produced by equal channel angular rolling at room temperature*, Mater. Charac., **58**, *7*, pp. 617–622, 2007.
19. HAMA, T., MAYAMA, T., TAKUDA, H., *Deformation behavior of a magnesium alloy sheet with random crystallographic orientations*, Key Eng. Mater., **611–612**, pp. 27–32, 2014.
20. KUWABARA, T., KUMANO, Y., ZIEGELHEIM, J., KUROSAKI, I., *Tension-compression asymmetry of phosphor bronze for electronic parts and its effect on bending behavior*, Int. J. Plast., **25**, *9*, pp. 1759–1776, 2009.

21. STAROSELSKY, A., ANAND, L., *A constitutive model for hcp materials deforming by slip and twinning: application to magnesium alloy AZ31B*, Int. J. Plast., **19**, *10*, pp. 1843–1864, 2003.
22. PROUST, G., TOME, C.N., JAIN, A., AGNEW, S.R., *Modeling the effect of twinning and detwinning during strain-path changes of magnesium alloy AZ31*, Int. J. Plast., **25**, *5*, pp. 861–880, 2009.
23. WANG, H., WU, P.D., TOME, C.N., WANG, J., *A constitutive model of twinning and detwinning for hexagonal close packed polycrystals*, Mater. Sci. Eng. A, **555**, pp. 93–98, 2012.
24. LEVESQUE, J., INAL, K., NEALE, K.W., MISHRA, R.K., *Numerical modeling of formability of extruded magnesium alloy tubes*, Int. J. Plast., **26**, *1*, pp. 65–83, 2010.
25. HAMA, T., TAKUDA, H., *Crystal-Plasticity Finite-Element Analysis of Inelastic Behavior During Unloading in a Magnesium Alloy Sheet*, Int. J. Plast., **27**, *7*, pp. 1072–1092, 2011.
26. HAMA, T., TAKUDA, H., *Crystal Plasticity Finite-Element Simulation of Work-Hardening Behavior in a Magnesium Alloy Sheet under Biaxial Tension*, Comput. Mater. Sci., **51,** pp. 156–164, 2012.
27. HAMA, T., TAKUDA, H., *Crystal plasticity finite-element simulation of deformation behavior in a magnesium alloy sheet considering detwinning*, Steel Res. Int., Special Edition, pp. 1115–1118, 2012.
28. HAMA, T., KITAMURA, N., TAKUDA, H., *Effect of twinning and detwinning on inelastic behavior during unloading in a magnesium alloy sheet*, Mater. Sci. Eng. A, **583**, pp. 232–241, 2013.
29. GRAFF, S., BROCKS, W., STEGLICH, D., *Yielding of magnesium: From single crystal to polycrystalline aggregates*, Int. J. Plast., **23**, *12*, pp. 1957–1978, 2007.
30. VAN HOUTTE, P., *Simulation of the rolling and shear texture of brass by the Taylor theory adapted for mechanical twinning*, Acta Metall., **26**, *4*, pp. 591–604, 1978.
31. HAMA, T., NAGATA, T., TEODOSIU, C., MAKINOUCHI, A., TAKUDA, H., *Finite-element simulation of springback in sheet metal forming using local interpolation for tool surfaces*, Int. J. Mech. Sci., **50**, *2*, pp. 175–192, 2008.
32. PEIRCE, D., ASARO, R.J., NEEDLEMAN, A., *Material rate dependence and localized deformation in crystalline solids*, Acta Metall., **31**, *12*, pp. 1951–1976, 1983.
33. YAMADA, Y., YOSHIMURA, N., SAKURAI, T., *Plastic stress-strain matrix and its application for the solution of elastic-plastic problems by the finite element method*, Int. J. Mech. Sci., **10**, *5*, pp. 343–354, 1968.
34. KAWKA, M., MAKINOUCHI, A., *Shell-element formulation in the static explicit FEM code for the simulation of sheet stamping*, J. Mater. Process. Technol., **50**, pp. 105–115, 1995.
35. BANU, M., TAKAMURA, M., HAMA, T., NAIDIM, O., TEODOSIU, C., MAKINOUCHI, A., *Simulation of springback and wrinkling in stamping of a dual-phase steel rail-shaped part*, J. Mater. Process. Technol., **173**, *2*, pp. 178–184, 2006.
36. HAMA, T., HOSOKAWA, N., TAKUDA, H., *Accurate parameter identification for crystal plasticity finite-element analysis in a magnesium alloy sheet*, NUMISHEET2014, Melbourne, Australia, January 6–10, 2014.
37. NAKAURA, Y., WATANABE, A., OHORI, K., *Grain refinement of AZ31 magnesium alloy sheets fabricated by rolled and heat treated twin roll cast plate* (in Japanese), J. Japan Inst. Light Metals, **58**, *1*, pp. 22–26, 2008.
38. HAMA, T., TAKUDA, H., *Work-hardening behavior upon reverse loading in a rolled AZ31 magnesium alloy sheet*, Key Eng. Mater., **622–623**, pp. 603–608, 2014.
39. MANN, G.E., SUMITOMO, T., CACERES, C.H., GRIFFITHS, J.R., *Reversible plastic strain during cyclic loading-unloading of Mg and Mg-Zn alloys*, Mater. Sci. Eng. A, **456**, pp. 138–146, 2007.
40. ANDAR, M.O., KUWABARA, T., STEGLICH, D., *Material modeling of AZ31 Mg sheet considering variation of r-values and asymmetry of the yield locus*, Mater. Sci. Eng. A, **549**, pp. 82–92, 2012.
41. CAZACU, O., PLUNKETT, B., BARLAT, F., *Orthotropic yield criterion for hexagonal closed packed materials*, Int. J. Plast., **22**, *7*, pp. 1171–1194, 2006.